GRAVITY WAVES AND THEIR EFFECTS FROM THE MARTIAN TROPOSPHERE TO THERMOSPHERE

A. S. Medvedev, *Max Planck Institute for Solar System Research, Göttingen,, Germany (medvedev@ mps.mpg.de)*, **E. Yiğit**, *George Mason University, Fairfax,USA*, **T. Kuroda**, *National Institute of Information and Communications Technology, Tokyo, Japan,* **Ch. Mockel**, *Max Planck Institute for Solar System Research, Göttingen,, Germany,* **P. Hartogh**, *Max Planck Institute for Solar System Research, Göttingen, Germany*.

Introduction:

Internal gravity waves (GWs) are an important mechanism of transporting energy and momentum between atmospheric layers in stably stratified planetary atmospheres. They are an essential part of the terrestrial climate [Yiğit and Medvedev, 2015]. Observations and theory/modeling indicate that GWs of tropospheric origin play a similar significant role on the middle and upper atmosphere of Mars. They affect the global circulation, thermal state; facilitate CO_2 ice cloud formation in the middle atmosphere, strongly influence the dynamics of the thermosphere. We present the recent developments in studies of GWs and their effects performed at Max Planck Institute in close collaboration with colleagues at other international institutions.

Gravity wave parameterization:

GWs of interest have horizontal scales usually smaller than the resolution of general circulation models and, thus, their effects have to be parameterized. Such parameterizations solve equations for the vertical evolution of GW variances or co-variances $\overline{u'w'}$ rigorously accounting for dissipation, breaking and filtering harmonics from the given ("source") spectrum at the lower boundary in the troposphere, e.g. [Yiğit et al., 2009, Medvedev et al., 2011]:

$$\frac{d\overline{u'w'}}{dz} = \left(\frac{1}{H} - \beta\right)\overline{u'w'},$$

where H is the scale height and β is the GW dissipation. Two issues must therefore be resolved: (a) defining β from the first principles [Yiğit et al., 2009] and (b) specifying source spectra $\overline{u'w'}(z = z_0)$. The latter is the subject of the extensive ongoing Earth climate study. On Mars, this goal will not be reached soon.

High resolution simulations:

To circumvent the problem of uncertainty in the detailed for of the source spectrum, a high-resolution (GW-resolving) GCM has been used [Kuroda et al., 2015; 2016] (see talk by T. Kuroda). The approach is based on the assumption that comprehensive GCMs can capture a significant portion of GWs and their sources. The model was run at the T106 spectral resolution (equivalent of ~1.1^0, or ~67 km).

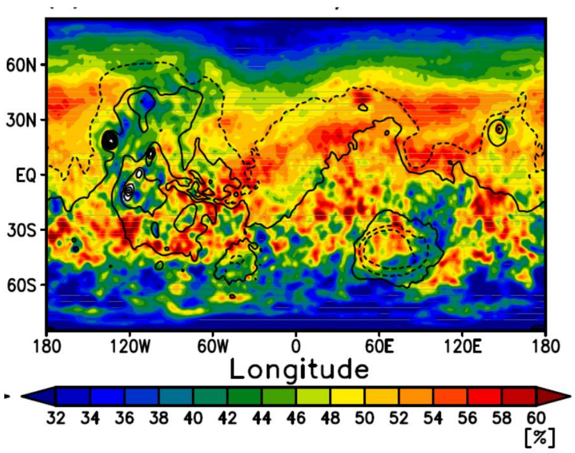

Figure 1. Percentage of the short-scale GW energy in the total energy simulated at p=260 Pa between L_s=270^0 and 300^0. Adapted from Kuroda et al. [2016].

As an example, Fig. 1 presents the distribution of small-scale GW activity (as a percentage of the total wave energy) in the troposphere. It directly simulates an enhanced GW generation in low latitudes, which was first derived from MGS radio occultation data [Creasey et al., 2006]. A global view of GW fields in the lower and middle atmosphere and the detailed analyses of their effects are given in the talk of T. Kuroda

GW-induced CO_2 ice clouds:

CO_2 ice clouds have been numerously detected in the middle atmosphere (50-100 km). Because the middle atmosphere is not cold enough to sustain condensation permanently, it was speculated that patches of cold air can be produced occasionally by temperature fluctuations associated with GWs and tides. This hypothesis has been further supported by a mesoscale modeling study [Spiga et al., 2012].

The MPI-MGCM (or MAOAM MGCM) with the implemented GW parameterization of Yiğit et al. [2008] has been used to simulate a global distribution of CO_2 ice clouds [Yiğit et al., 2015]. The criterion for condensation is $T - |T'| \leq T_s$, where T' is the fluctuation of temperature T (from the parameterization) and T_s is the subsaturation temperature at a given pressure.

Figure 2 presents a zonal mean and 40-sol average of the zonal mean temperature (contours), temperature fluctuations (reddish shading) and the probability of reaching conditions for CO_2 ice formation.

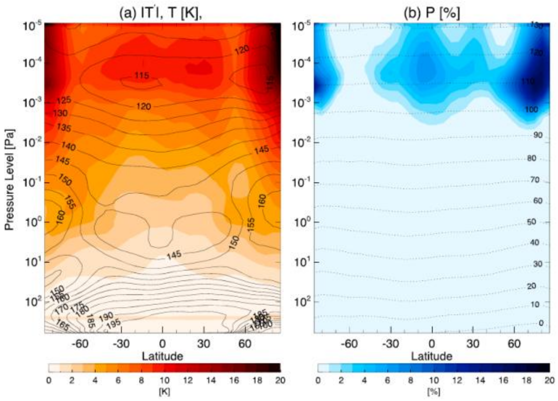

Figure 2. (a) Zonal mean temperature (contours), GW-induce temperature fluctuations (color shades). (b) Probability of CO2 ice formation (shades), and approximate height (contours). Adapted from [Yiğit et al., 2015].

An example of more detailed simulations (around $Ls=20^0$ is given in Figure 3. The probability is highest in polar regions. Many clouds are formed in low latitude middle atmosphere. Also, simulations predict a probability of cloud formation in high-latitude lower thermosphere (not yet observed).

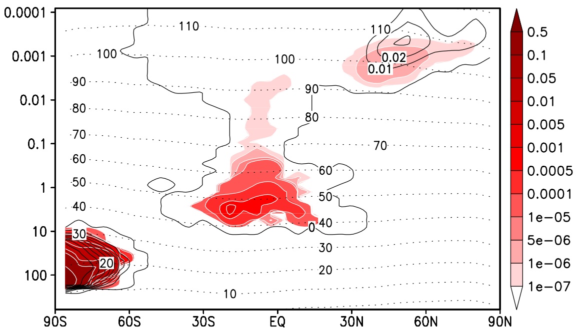

Figure 3. Color shading shows the ratio of resolved CO2 ice clouds to the maximum amount of ice (in kg). Contour lines show a probability of CO2 ice formation if GW-induced fluctuations of *T'* are accounted for.

For more details on GW effects on CO_2 cloud formation see the talk by E. Yiğit.

GW-induced cooling:

In a freely propagating GW, oscillations of *T'* and vertical velocity *w'* are in opposite phase, and $\overline{w'T'} = 0$. Dissipation introduces a phase shift and the sensible heat flux is no longer zero. $\overline{w'T'}$ is always negative (directed downward), and the associated heating cooling rate is $-\rho^{-1}d(\rho\overline{w'T'})$/dz. Thus, dissipating/breaking GWs transport heat down providing cooling above the dissipation level and heating below.

In Earth's thermosphere, GW-induced cooling is the second (after molecular heat conduction) cooling factor [Yiğit and Medvedev, 2009]. On Mars, GW-induced cooling is of similar importance [Medvedev and Yiğit, 2012].

A comparison of GW cooling with that due to radiative transfer in CO_2 15 mkm IR bands have been performed in the work by [Medvedev et al., 2015]. Figure 4 shows the difference between the zonal mean temperature simulated with and without GW cooling included. It is seen that GWs produce by up to 20 K colder temperatures in the mesosphere and lower thermosphere (MLT), especially in high latitudes.

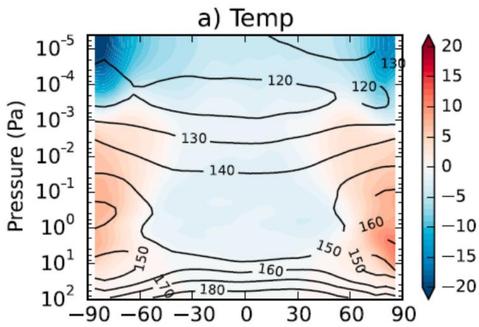

Figure 4. MPI-MGCM-simulated zonal-mean temperature simulated with GW effects included (contours). Color shades show the difference with the similar run, but without GWs. Adapted from [Medvedev et al., 2015]

A comparison of cooling rates due to the 15 mkm CO_2 IR transfer and GWs is given in Figure 5.

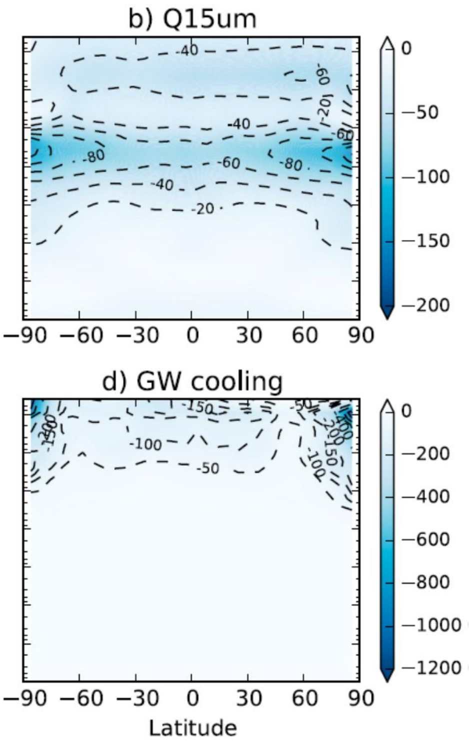

Figure 5. (b) 15 mkm CO_2 cooling rates (contours and shades). (d) GW-induced cooling rates. Adapted from [Medvedev et al., 2015]

The results show that (a) both mechanisms produce a colder simulated MLT; (b) GW effects take place, generally, higher than CO_2 radiation; (c) within the current uncertainties with distributions of [O] and GW sources, the effects of both cooling mechanisms are similar, and (d) further measurements are required to constrain both mechanisms for models.

Use of MAVEN observations:

Imaging Ultraviolet Spectrograph (IUVS) onboard MAVEN measures the far and mid-UV airglow, from which vertical profiles of density are retrieved (between 130 and 190 km). We performed a comparison of the retrieved CO_2 density with MGCM simulations [Medvedev et al., 2016]. Figure 6 presents the ratio of the simulated and observed densities for three latitudinal bins around L_s~217^0. Different color lines are for different model scenarios. The latter included different input [O] profiles, solar activity, GW setup. It is seen that the majority of simulations match observations within one standard deviation.

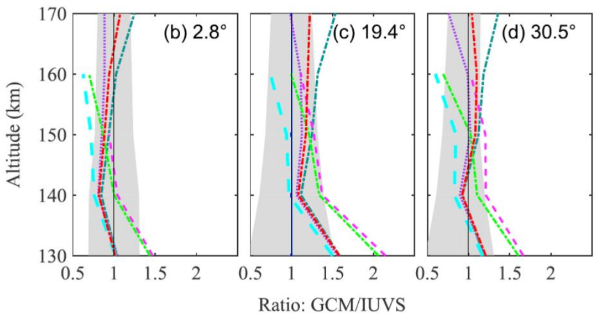

Figure 6. Ratios between modeled and observed zonal mean CO_2 number density. Gray shading represents 1 standard deviations of observations $\pm\sigma$.

A comparison of the simulated and retrieved CO_2 temperature gives more conclusive results (Figure 7). In the periods of high solar activity, as during the IUVS/MAVEN measurements, the mean effect of GWs is to heat the thermosphere in low latitudes and cool down in middle and high latitudes. The simulations that did not account for GWs produced systematically colder temperature. In Figure 7, thus simulated temperature profiles do not match observations within one standard deviation (gray shades).

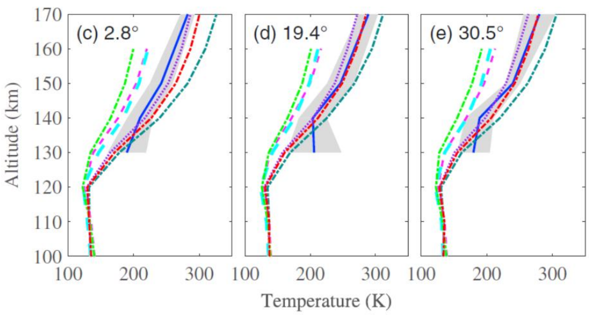

Figure 7. Simulated temperature profiles (contours) for various scenarios. Gray shading presents one sigma variations. Those systematically colder profiles are for runs that did not include parameterized GWs.

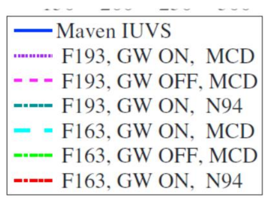

Figure 8. List of modeling scenarios presented in Figs. 6 and 7. F193 and F163 are for the $F_{10.7}$ flux, MCD and N94 are for the Mars Climate Database and [Nair, 1994] oxygen scenarios, GW ON and GW OFF indicate turning on and off effects of parameterized GWs.

For more comparisons, see talk by Ch. Mockel.

Summary:

Gravity waves play a significant role in the momentum and energy budget of the middle and upper atmosphere of Mars. We have presented some key highlights on the recent developments in GW studies based on our Martian general circulation modeling incorporating a state-of-the-art GW parameterization, high-resolution general circulation modeling, and MAVEN observations. GW sources are highly variable in the lower atmosphere. A broad spectrum of GWs propagates into the mesosphere and thermosphere, providing appreciable heating/cooling, which ultimately facilitate CO_2 ice cloud formation. Comparison of the MGCM with recent MAVEN observations provide further evidence that GW processes should be adequately represented in models in order to better reproduce Martian observations.

References:

Kuroda, T., A. S. Medvedev, E. Yiğit, and P. Hartogh (2015), Geophys. Res. Lett., 42, 9213-9222, doi:10.1002/2015GL066332.

Kuroda, T., A. S. Medvedev, E. Yiğit, and P. Hartogh (2016), J. Atmos. Sci, early online release.

Medvedev, A. S., and E. Yiğit (2012), Geophys. Res. Lett., 39, L05201, doi:10.1029/2012GL050852.

Medvedev, A. S., F. González-Galindo, E. Yiğit, A. G. Feofilov, F. Forget, and P. Hartogh (2015), J. Geophys. Res. Planets, 120, 913–927, doi: 10.1002/ 2015JE004802.

Medvedev, A. S., H. Nakagawa, C. Mockel, E. Yiğit, T. Kuroda, P. Hartogh, et al., (2016). Geophys. Res. Lett., 43, 3095–3104, doi:10.1002/2016 GL068388.

Medvedev, A. S., E. Yiğit, P. Hartogh, and E. Becker (2011), J. Geophys. Res., 116, doi:10.1029/ 2011JE003848.

Yiğit, E., and A. S. Medvedev (2015), Adv. Space Res., 55, 983-1003, doi:10.1016/j.asr.2014.11. 020.

Yiğit, E., A. S. Medvedev, A. D Aylward, P. Hartogh, and M. J. Harris (2009),. J. Geophys. Res., 114, D07101, doi:10.1029/2008JD011132.

Yiğit, E., A. S. Medvedev, and P. Hartogh (2015), Geophys. Res. Lett., 42, 4294–4300, doi:10.1002 /2015GL064275.